Journal of Power Sources 189 (2009) 480–484

Contents lists available at ScienceDirect

Journal of Power Sources

journal homepage: www.elsevier.com/locate/jpowsour

Short communication

Improvement of cycling stability of Si anode by mechanochemcial reduction and carbon coating

Y. Liu[a,*], Z.Y. Wen[a,*], X.Y. Wang[a], X.L. Yang[b], A. Hirano[c], N. Imanishi[c], Y. Takeda[c]

[a] Shanghai Institute of Ceramics, Chinese Academy of Sciences, 1295 Ding Xi Road, Shanghai 200050, PR China
[b] College of Mechanical and Material Engineering, Three Corges University, 8 Daxue Road, Yichang 443002, PR China
[c] Department of Chemistry, Faculty of Engineering, Mie University, Kamihama-cho, Tsu, Mie 514-8507, Japan

ARTICLE INFO

Article history:
Received 2 July 2008
Received in revised form 8 November 2008
Accepted 11 December 2008
Available online 24 December 2008

Keywords:
Lithium ion batteries
Anode
Silicon
Mechanochemical reduction
Cycling stability

ABSTRACT

In this work, a novel composite consisting of nanosized silicon highly dispersed within the porous, elastic and conductive oxide/carbon matrix has been developed as an anode candidate for lithium ion batteries. The composite was prepared by a mechanochemical reaction between SiO and Li under ball milling followed by a carbon coating using the pyrolysis of poly(vinyl chloride)–co-vinyl acetate. The porous structure can effectively suppress the volume change of silicon during the electrochemically Li-alloying process. No obvious capacity fading was observed up to 100 cycles with a stable capacity of 620 mAh g^{-1}. The factors influencing the microstructure and the electrochemical behavior of the composite were discussed.

1. Introduction

Due to the largest capacity among all known Li-storage hosts, silicon is an attractive anode alternative for the commercial graphite for Li-ion batteries. However, it shows a rapid capacity fading during cycling because of the strong volume change. This, in turn, seriously hinders its practical applications. An effective approach to solve this problem is to create a composite microstructure comprising active silicon uniformly dispersed in an inert matrix [1–9]. Additionally, it is essential to reduce the particle size of Si to nanoscale. Various techniques such as gas-phase evaporation [10], high temperature aerosol reaction [11], co-sputtering [12], Si ion implantation [13], electrochemical etching [14] and ball-milling [15], have been investigated to synthesize the nanosized Si. Among them, the ball-milling technique is a cost-effective method for producing nanosized Si in large scale. The nanosized Si can be produced by ball-milling of graphite and SiO_2 powders for 10 days followed by an annealing treatment [16]. It was also shown that the nanosized Si particles embedded in a solid matrix of amorphous Al_2O_3 and SiO_2 can be obtained by the mechanochemical reaction, a solid-phase redox process, between SiO_2 and Al powders under ball-milling [17]. More recently, Sandu et al. reported the production of nanosized Si via the reaction between $SiBr_4$ solution and Mg granules during the ball-milling process [18]. The Si source and the reducing agent are two key factors for the mechanochemical reaction under ball-milling. Compared with SiO_2 and $SiBr_4$, SiO is an attractive Si source since it has much lower bonding energy between Si and O. Previous study indicated that the nanosized Si can be obtained by ball-milling SiO and Li with graphite as a dispersant [19]. Zheng et al. also reported a nano-porous Si/graphite composite using Al as the reducing agent under two-step ball-milling followed by an etching process [20]. The nanosized Si can be embedded with the carbonaceous matrix using the pyrolysis to obtain a better performance. Morita and Takami in Toshiba group developed a nanosilicon cluster-SiO_x–C composite by ball-milling the mixture of SiO and graphite followed by a carbon coating using a pyrolysis of the polymerized furfuryl alcohol [21]. The composite had a capacity over 700 mAh g^{-1} and a long cycle life.

In this work, a porous Si/Li_2O/C composite was developed by a mechanochemical reaction between SiO and Li under ball-milling followed by a carbon coating using the pyrolysis of poly(vinyl chloride)–co-vinyl acetate. Electrochemical properties and microstructures of the composite were investigated systematically.

2. Experimental

2.1. Preparations of the Si based composites

Planetary Mono Mill P-5 (Fritsch, Germany) using an 80 ml alumina vial filled with 15 alumina balls of 10 mm in diameter was used for the milling. For the preparation of the Si/Li_2O composite,

* Corresponding authors. Tel.: +86 21 5241 2272; fax: +86 21 5241 3903.
E-mail addresses: yuliu@mail.sic.ac.cn (Y. Liu), zywen@mail.sic.ac.cn (Z.Y. Wen).

0378-7753/$ – see front matter © 2009 Elsevier B.V. All rights reserved.
doi:10.1016/j.jpowsour.2008.12.045

silicon monoxide (SiO, 99.99%, Aldrich) and lithium metal with a molar ratio of 5:6 were transferred to the alumina vial inside an argon-filled glove box (VAC) for mechanical milling (475 rpm). The mass ratio of the milling balls to the reactants was 10:1. Direct ball-milling of SiO with lithium metal led the formation of clumps of the powder due to the low melting point of lithium (mp 180.1 °C). Thus, a lubricant was added. The milling time was 5 h. For the comparison, the Si/Al_2O_3 composite was prepared by milling a mixture of SiO and aluminum (200 mesh, 99.99%) powders with a molar ratio of SiO:Al = 3:2 at the speed of 500 rpm for 15 h. The obtained Si/Li_2O composite was added into the solution in which poly(vinyl chloride)–co-vinyl acetate (Aldrich) was dissolved in tetrahydrofuran solution. It was homogeneously mixed under ultrasonic action. The weight ratio of the Si/Li_2O composite to the organic precursor was 3:7. The solvent evaporated under stirring to get a solid blend. The blend precursor was then gradually heated to 900 °C under Ar/H_2 (4% H_2) atmosphere. After pyrolysis at 900 °C for 2 h, the furnace was cooled naturally. The products were further ground. Nanosized $SiO_{1.1}$ (ca. 50 nm) and nanosized Si (ca. 60 nm) were commercially available. Powder X-ray diffraction (XRD) patterns were obtained using automated powder diffractometer with Cu K_α radiation (Rotaflex RU-200B, Rigaku-denki Corporation). The morphology of the materials was characterized with scanning electron microscopy (SEM) and transmission electron microscopy (TEM).

2.2. Cell assembly and electrochemical tests

The electrode containing 8 wt% acetylene black (AB), 80 wt% active materials and 12 wt% Poly(vinylidene fluoride) (PVDF) was prepared by a dry process. The active powders and AB were homogeneously mixed with PVDF, and the mixture was pressed onto a 300-μm thick Ni foam, which served as a current collector. After pressing, the geometric area of the electrodes was 1.0 cm^2, and the typical thickness was 190–200 μm. To evaluate the electrochemical properties of the electrodes, a half-cell containing $LiClO_4$/EC + DMC (ethylene carbonate plus diethyl carbonate as 1:1 in volume) electrolyte was used, and lithium metal was utilized as the counter electrode. All the three layers, including test electrode, separator and lithium metal, were stacked in a 2025 coin type cell in a glove box. Unless stated elsewhere, cycling was carried out at a constant current density of 0.18 mA mg^{-1} and a voltage cutoff at 1.5/0.02 V vs. Li/Li^+. Charge and discharge of the cells refer, respectively, to lithium extraction from and insertion into the active hosts. Electrode capacity was calculated according to the weight of active materials. The cyclic voltammetry experiments were performed on a CHI440 Electrochemical Workstation.

3. Results and discussion

3.1. Nanosized Si prepared by mechanochemical reduction

The XRD patterns of the SiO powders, thermally decomposed SiO, nanosized $SiO_{1.1}$ powder, milled Si/Al_2O_3 and Si/Li_2O composites were shown in Fig. 1. The peaks of Si, SiO and SiO_2 were distinguished. The SiO powders showed an obvious peak at approximately 26°, reflecting a high crystallization feature. After the thermal treatment at 900 °C, the SiO completely decomposed to SiO_2 and Si. It showed the weak and broad peaks. The nanosized $SiO_{1.1}$ contains a small amount of SiO_2 besides the amorphous SiO and the crystalline silicon [22]. For the Si/Al_2O_3 composite, the peak trace of SiO was observed. It indicates that the mechanochemical reaction between SiO and Al under ball-milling did not perform completely. In contrast, the milled Si/Li_2O composite was almost amorphous. Compared with Al, Li is relatively easy to reduce SiO due to a higher negative free energy change. Yang et al. have reported

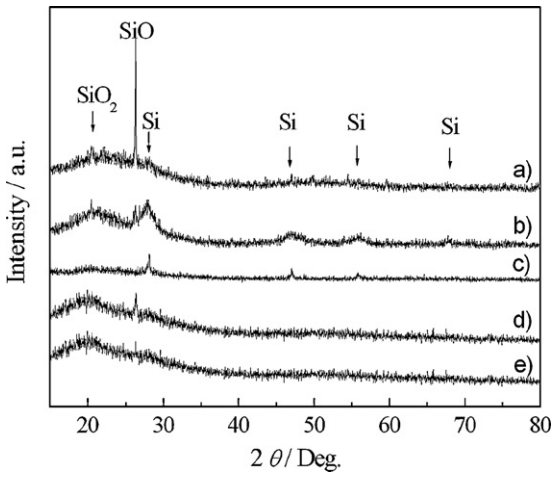

Fig. 1. XRD patterns of the (a) SiO, (b) thermally decomposed SiO at 900 °C under Ar, (c) $SiO_{1.1}$, (d) ball-milled Si/Al_2O_3 and (e) ball-milled Si/Li_2O composites.

the observation of the formation of the amorphous oxides besides Si under ball-milling of SiO with Li according to the reaction: $5SiO + 6Li \rightarrow Li_2O + Li_4SiO_4 + Si$ [19]. Zheng et al. also demonstrated that the mechanochemical reduction of SiO by Al mainly leads to an amorphous Al_2O_3 and crystalline Si based on the reaction: $SiO + Al \rightarrow Si + Al_2O_3$ [20]. This is consistent with the present study. Here, the composite obtained from SiO and Li was named as Si/Li_2O, not Si/Li_4SiO_4–Li_2O, for the sake of convenience. It was considered that the amorphous Si in the XRD patterns was mainly due to the influence of the milling conditions.

Fig. 2 shows the SEM micrograph of the milled Si/Li_2O composite. The large agglomerates contained many small spherical particles in 3–6 μm size, as shown in Fig. 2a. This was due to the repeated fracturing and rewelding processes of the powders induced by the strong ball-to-powder collisions. Fig. 2c further shows the high-resolution transmission electron microscope (HRTEM) image of the product. As found, nanosized Si domains (several nm) was uniformly dispersed in the amorphous oxide.

As reported, nanosized $SiO_{1.1}$ has a voltage/capacity curve similar with SiO. It shows the best cycling performance among all the active silicon oxides [22]. Fig. 3 shows the charge and discharge profiles of the $SiO_{1.1}$ and the milled Si/Li_2O electrodes. At the first cycle shown in Fig. 3a, a small voltage plateau at 0.6 V was observed for $SiO_{1.1}$. It corresponds to the electrochemical transformation of SiO to Si. Below 0.1 V, a flat voltage plateau was obvious in the Li-intercalation stage. It was attributed to an irreversible phase transformation of silicon from crystalline to amorphous. It resulted in an obvious shift in the discharge voltage from the first cycle to the subsequent cycles, as shown in Fig. 3b. In contrary, the slope observed in the voltage plateau for the Si/Li_2O composite indicated that the discharge started directly from an amorphous or microcrystalline state of Si. This is in good agreement with the XRD observations. The discharge voltage of the $SiO_{1.1}$ electrode showed a decrease of ca. 0.1–0.3 V compared with the Si/Li_2O composite, as shown in Fig. 3b. It is attributed to a higher voltage polarization due to the inactive SiO_2. The 1st efficiency of the Si/Li_2O and the $SiO_{1.1}$ composites was 89% and 42%, respectively. The first cycle efficiency of the Si/Li_2O composite obtained here is obviously higher than that (ca. 81%) of the nanosized Si/Li/O composite prepared by a similar method [19]. It is mainly due to the difference in the experimental conditions of the mechanochemical reaction.

For a comparison, Al metal was used as the reducing agent for the mechanochemical reduction of SiO under ball-milling. Fig. 4 shows the charge and discharge profiles of the Si/Al_2O_3 composite. The voltage curves were similar with those of the Si/Li_2O compos-

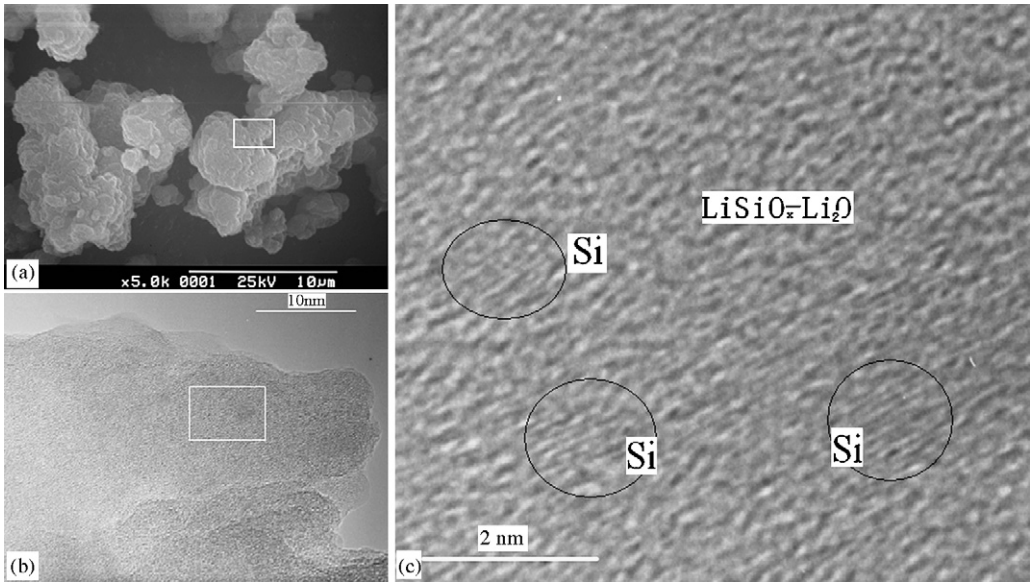

Fig. 2. (a) SEM micrograph of the milled Si/Li_2O composite, (b) SEM micrograph of the enlarged section of (a) and (c) FRTEM image of the enlarged section of (b).

ite. However, the efficiency at the first cycle was approximately 70%, which was much lower than that of the Si/Li_2O composite. It is attributed to the incomplete reaction of SiO and Al. Further optimization on the milling conditions will be necessary.

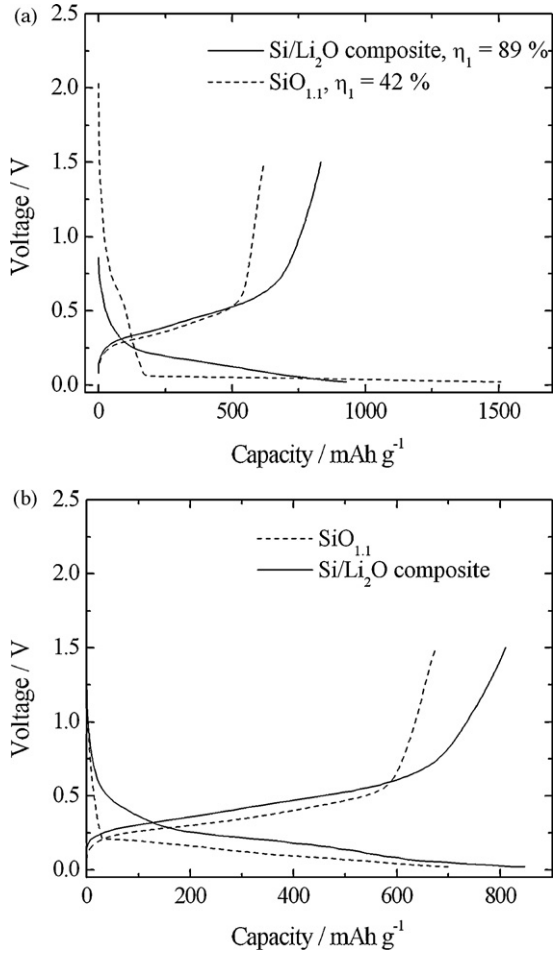

Fig. 3. Charge and discharge profiles of Si/Li_2O and $SiO_{1.1}$ in (a) the first cycle and (b) the second cycle.

Fig. 5 shows the cyclic voltammograms (CV) of the Si/Li_2O composite and the SiO electrodes. The major difference between the two electrodes is the reduction curve at the first cycle. Two obvious peaks at approximately 0.1 and 0 V as well as a broad peak at 0.6 V were observed for the SiO electrode. It was considered that the 0.6 V peak is related with the irreversible reduction of SiO to be Si. The peaks at 0.1 and 0 V mainly corresponded to the formation of Li-alloys like $Li_{12}Si_7$ and $Li_{22}Si_5$ phases. Nagao et al. reported that the metallic silicon clusters are finely dispersed in the SiO_4 tetrahedral network for the SiO structure [23]. This can explain the electrochemically kinetic behavior of SiO at the first reduction scan. In contrast, only one reduction peak at around 0 V was observed for the Si/Li_2O composite at the first cycle. This behavior is highly similar to that of pure Si. It indicates the electrochemical Li–Si alloying reaction [24]. From the second cycle, no obvious difference was observed for the SiO and the Si/Li_2O composites. It suggests that the inserted lithium can reversibly react with silicon to form the Li–Si alloys. The curves highly overlapped during the redox reactions after the second cycle.

Fig. 6 shows the cycling performance of different Si-based materials. The cycling stability of the $SiO_{1.1}$ and the Si/Li_2O composites

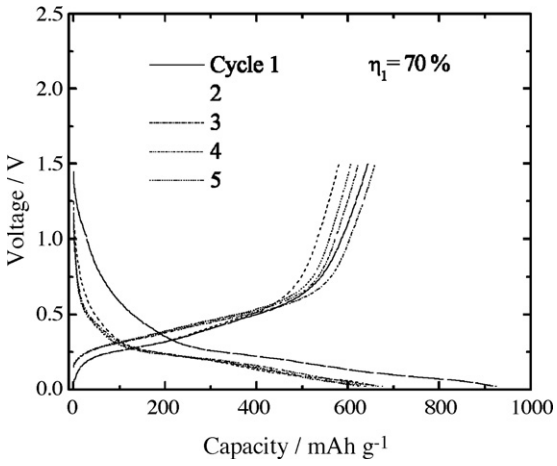

Fig. 4. Charge and discharge profiles of the milled Si/Al_2O_3 composite for different cycles.

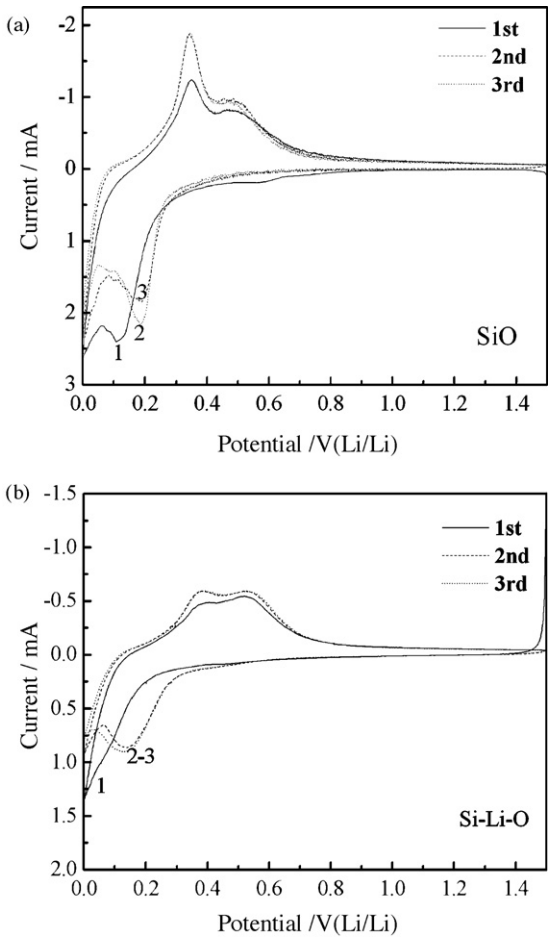

Fig. 5. Cyclic voltammograms of (a) the SiO and (b) Si/Li_2O composite from cycle 1 to cycle 3 at the scan rate of 0.05 mV s^{-1} with the voltage range of 0–1.5 V vs. Li/Li^+.

was obviously superior to that of pure Si. After 40 cycles the initial capacity remained 68.4% and 69% for the $SiO_{1.1}$ and the Si/Li_2O composites, respectively. This is related to the volume expansion during Li-accumulation. It was considered that the volume change of Li–Si alloy will be approximately 400% when 1 mol Si absorbed 4.4 mol Li [25]. In contrast, the volume change of the "SiO to Li–silicate" is only half as great as that of the "Si to Li–Si alloy" according to a research by Miyachi et al. [26]. The lithium utilization and the volume change

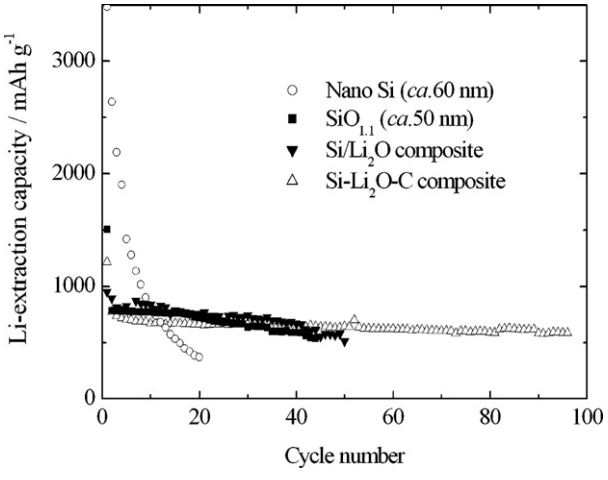

Fig. 6. Comparison in the cycling performance of the nanosized Si, $SiO_{1.1}$, Si/Li_2O composite and $Si/Li_2O/C$ composite.

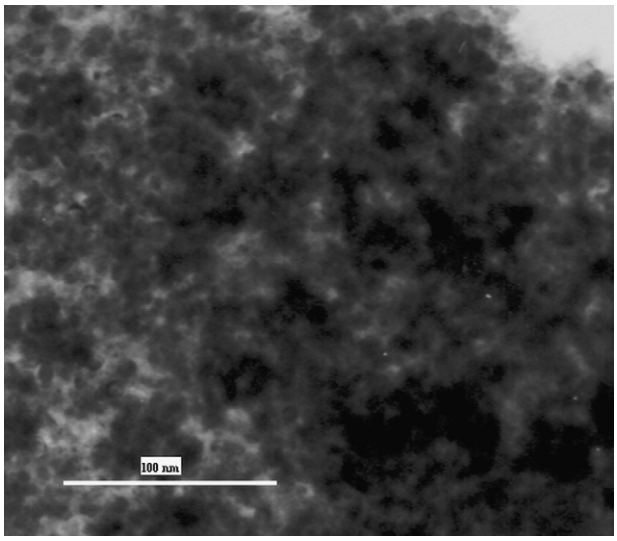

Fig. 7. SEM micrograph of the pyrolyzed $Si/Li_2O/C$ composite.

of the $SiO_{1.1}$ and the Si/Li_2O composites were thus much less than those of pure Si. Moreover, the inert Li–silicate phase formed in the $SiO_{1.1}$ and the Si/Li_2O composites can effectively alleviate the volume change of Si. This results in a better performance over the nanosized Si.

3.2. Preparation of a porous $Si/Li_2O/C$ composite

The nanosized Si/Li_2O composite can control the volume change of the Li–Si reaction. However, the cyclability was not satisfactory. An ideal morphology will create a porous structure in which the interspaces can effectively absorb the volume expansions of the Li–Si alloying reaction. Fig. 7 shows the SEM image of the $Si/Li_2O/C$ composite. It was obtained by dispersing the Si/Li_2O particles within the pyrolyzed carbon. The pores with diameter from 5 to 10 nm may arise from the decomposition of the poly(vinyl chloride)–co-vinyl acetate during the pyrolysis.

Fig. 8 shows the charge and discharge profiles of the pyrolyzed $Si/Li_2O/C$ composite. Compared with those of the $SiO_{1.1}$ and Si/Li_2O composites, the contribution of the reversible capacity are mainly due to the electrochemically Li–Si alloying reaction. This led to a high capacity of approximately 620 mAh g^{-1}. However, the porous structure will increase the contacting area of some nansozied Si particles with the electrolyte. The voltage plateau at 0.9–0.5 V cor-

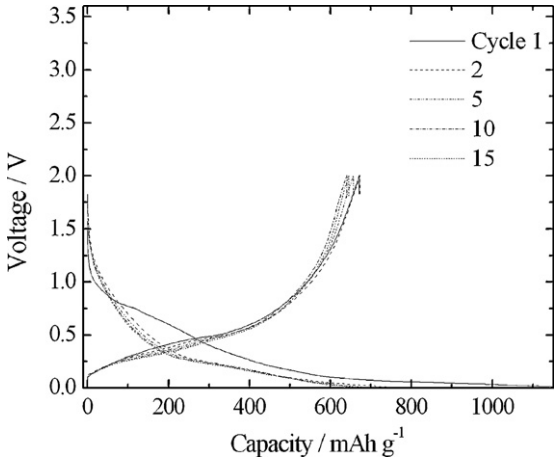

Fig. 8. Charge and discharge profiles of the pyrolyzed $Si/Li_2O/C$ composite.

responded to the amorphous carbon. It also greatly increased the irreversible capacity at the first cycle. As a result, the columbic efficiency at the first cycle was decreased to 60%.

Cycling performance of the porous $Si/Li_2O/C$ composite was shown in Fig. 6. No obvious capacity fading was observed up to 100 cycles. The capacity fade rate was thus calculated to be less than 0.15% per cycle. The cycling performance of the porous $Si/Li_2O/C$ composite was obviously superior to that of the $SiO_{1.1}$ and the Si/Li_2O composites. It indicated that the silicon particles were highly fixed in the porous, conductive and elastic oxides/carbon phases. This could effectively suppress the pulverizing of Si by the volume change during cycling.

4. Conclusion

We have presented an effective way to obtain the porous $Si/Li_2O/C$ composite using the mechanochemical reaction between SiO and metallic Li under ball milling followed by a carbon coating via the pyrolysis of poly(vinyl chloride)–co-vinyl acetate. The composite showed better cycling stability than the nanosized $SiO_{1.1}$ (ca. 50 nm) and the nanosized Si (ca. 60 nm). No obvious capacity fade was observed up to 100 cycles with a reversible capacity of approximately 620 mAh g^{-1}. However, the columbic efficiency at the first cycle was lowered due to the exposed surface of the nanosized Si to electrolyte. Future work is required to eliminate this drawback for the practical applications.

Acknowledgments

This work was financially supported by NSFC Project No. 20333040 and 50672114, 863 Project of China No. 2006AA03Z232 and 973 Project of China No. 2007CB209700.

References

[1] II-S. Kim, P.N. Kumta, G.E. Blomgren, Electrochem. Solid-State Lett. 3 (2000) 493.
[2] J. Yang, B.F. Wang, K. Wang, Y. Liu, J.Y. Xie, Z.S. Wen, Electrochem. Solid-State Lett. 6 (2003) A154.
[3] Y. Liu, K. Hanai, T. Matsumura, N. Imanishi, A. Hirano, Y. Takeda, Electrochem. Solid-State Lett. 7 (2004) A492.
[4] B.C. Kim, H. Uono, T. Satou, T. Fuse, T. Ishihara, M. Ue, M. Senna, J. Electrochem. Soc. 152 (2005) A523.
[5] H.Y. Lee, S.M. Lee, Electrochem. Commun. 6 (2004) 465.
[6] Y. Zhang, X.G. Zhang, H.L. Zhang, Z.G. Zhao, F. Li, C. Liu, H.M. Cheng, Electrochim. Acta 51 (2006) 4994.
[7] M.K. Datta, P.N. Kumta, J. Power Sources 158 (2006) 557.
[8] M. Holzaptel, H. Buqa, F. Krumeich, P. Novak, F.-M. Petrat, C. Veit, Electrochem. Solid-State Lett. 8 (2005) A516.
[9] H. Uono, B.C. Kim, T. Fuse, M. Ue, J. Yamaki, J. Electrochem. Soc. 153 (2006) A1708.
[10] R. Okada, S. Iijima, Appl. Phys. Lett. 58 (1991) 1662.
[11] K.A. Littau, P.J. Szajowski, A.J. Muler, A.R. Kortan, L.E. Brus, J. Phys. Chem. 97 (1993) 1224.
[12] Y. Maeda, N. Tsukamoto, Y. Yazawa, Y. Kanemitsu, Y. Masumoto, Appl. Phys. Lett. 59 (1992) 3168.
[13] T. Shimizu, S. Nakao, K. Sayito, Appl. Phys. Lett. 65 (1994) 1814.
[14] M.H. Nayfeh, N. Barry, J. Therrien, O. Akcakir, E. Gratton, G. Belomoin, Appl. Phys. Lett. 78 (2001) 1131.
[15] T.D. Shen, I. Shmagin, C.C. Koch, R.M. Kolbas, Y. Fahmy, L. Bergman, R.J. Nemanich, M.T. McClure, Z. Sitar, M.X. Quan, Phys. Rev. B 55 (1997) 7615.
[16] C. Lam, Y.F. Zhang, Y.H. Tang, C.S. Lee, I. Bello, S.T. Lee, J. Cryst. Growth 220 (2000) 466.
[17] C. Araujo-Andrade, F.J. Espinoza-Beltran, S. Jimenez-Sandoval, J. Gonzalez-Hernandez, Scripta Mater. 49 (2003) 773.
[18] I. Sandu, P. Moreau, D. Guyomard, T. Brousse, L. Roué, Solid State Ionics 178 (2007) 297.
[19] X.L. Yang, Z.Y. Wen, X.X. Xu, B. Lin, S.H. Huang, J. Power Sources 164 (2007) 880.
[20] Y. Zheng, J. Yang, J. Wang, Y. NuLi, Electrochim. Acta 52 (2007) 5863.
[21] T. Moritaz, N. Takami, J. Electrochem. Soc. 153 (2006) A425.
[22] J. Yang, Y. Takeda, N. Imanishi, C. Capiglia, J.Y. Xie, O. Yamamoto, Solid State Ionics 152–153 (2002) 125.
[23] Y. Nagao, H. Sakaguchi, H. Honda, T. Fukunaga, T. Esaka, J. Electrochem. Soc. 151 (2004) A1572.
[24] Y. Liu, K. Hanai, J. Yang, N. Imanishi, A. Hirano, Y. Takeda, Solid State Ionics 168 (2004) 61.
[25] N. Yabuuchi, T. Mutoh, T. Ohzuku, Abstracts of the 44th Battery Symposium in Japan, Sakai, 2003, p. 438.
[26] M. Miyachi, H. Yamamoto, H. Kawai, T. Ohta, M. Shirakata, J. Electrochem. Soc. 152 (2005) A2089.